Magnetic Properties of the Layered Lanthanide Hydroxide Series Y$_x$Dy$_{8-x}$(OH)$_{20}$Cl$_4$·6H$_2$O: From Single Ion Magnets to 2D and 3D Interaction Effects

Bernardo Monteiro,[†] Joana T. Coutinho,[†] Cláudia C. L. Pereira,[†] Laura C. J. Pereira,*[,†] Joaquim Marçalo,[†] Manuel Almeida,[†] José J. Baldoví,[‡] Eugenio Coronado,[‡] and Alejandro Gaita-Ariño*[,‡]

[†]C²TN, Instituto Superior Técnico/CFMCUL, Universidade de Lisboa, Estrada Nacional 10, 2695-066 Bobadela LRS, Portugal
[‡]Instituto de Ciencia Molecular, Universitat de València, C/Catedrático José Beltrán 2, E-46980 Paterna, Spain

Ⓢ *Supporting Information*

ABSTRACT: The magnetic properties of layered dysprosium hydroxides, both diluted in the diamagnetic yttrium analogous matrix (LYH:0.04Dy), and intercalated with 2,6-naphthalene dicarboxylate anions (LDyH-2,6-NDC), were studied and compared with the recently reported undiluted compound (LDyH = Dy$_8$(OH)$_{20}$Cl$_4$·6H$_2$O). The Y diluted compound reveals a single-molecule magnet (SMM) behavior of single Dy ions, with two distinct slow relaxation processes of the magnetization at low temperatures associated with the two main types of Dy sites, 8- and 9-fold coordinated. Only one relaxation process is observed in both undiluted LDyH and intercalated compounds as a consequence of dominant ferromagnetic Dy−Dy interactions, both intra- and interlayer. Semiempirical calculations using a radial effect charge (REC) model for the crystal field splitting of the Dy levels are used to explain data in terms of contributions from the different Dy sites. The dominant ferromagnetic interactions are explained in terms of orientations of easy magnetization axes obtained by REC calculations together with the sign of the superexchange expected from the Dy−O−Dy angles.
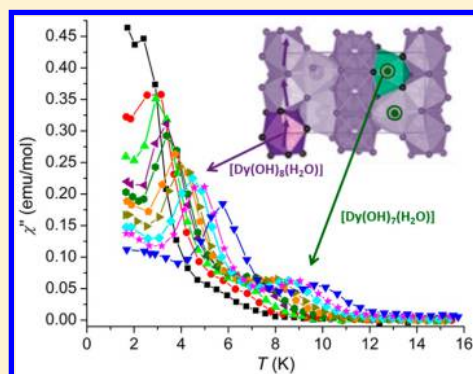
INTRODUCTION

There has been an increasing interest in layered metal hydroxides because of the unique combination of properties achieved by inserting a variety of anions in between the host inorganic layers. These lamellar hosts offer a broad range of possibilities,[1,2] such as introducing a stimulus responsive molecule that controls the physical properties of the host.[3,4] In this context, a particular class of materials is the so-called layered lanthanide hydroxides (LLHs),[5] which are compounds with a general chemical formula of Ln$_2$(OH)$_5$A·nH$_2$O, where A represents interlayer anions such as Cl$^-$, NO$_3^-$, Br$^-$, etc., and n is 1.5−1.8. The unit cell of these materials contains three crystallographically distinct lanthanide sites, with two different Ln environments, as shown in Figure 1. One of the Ln ions presents an 8-fold coordination, [Ln(OH)$_7$(H$_2$O)], in a dodecahedron environment, and two Ln ions present a 9-fold coordination, [Ln(OH)$_8$(H$_2$O)], forming a monocapped square antiprism coordination geometry with the capping position occupied by the water molecule. The crystal structure is built up along the c-axis via an alternative stacking of the host layer, composed of edge-shared [Ln(OH)$_7$(H$_2$O)] and [Ln-(OH)$_8$(H$_2$O)] polyhedra, with each hydroxyl acting as a μ_3-bridge connecting the lanthanide centers and the anions which are intercalated between the layers ensuring charge neutrality (Figure 1).[6] The small anions A in these structures can be easily replaced by more bulky ones following an intercalation process

which preserves the layered structure.[7] The compositional flexibility of such materials, where the identity of both cation and anion can be controlled to target a specific application, makes them extremely appealing for different possible applications, and studies have focused mainly on their optical properties.[8] The magnetic properties of these lanthanide compounds are also potentially interesting, but have been a lot more neglected in spite of their potential, namely for providing single molecule behavior with large anisotropy barriers[9] and high blocking temperatures.[10]

The study of the magnetic properties of LLHs has been essentially restricted to our recent report on the magnetic properties of Dy$_8$(OH)$_{20}$Cl$_4$·6H$_2$O (LDyH) revealing the presence of slow magnetic relaxation at low temperatures with a blocking temperature of 3 K and an energy barrier of 36.1 K, with a behavior typical of single molecule magnets.[11] This was the first example of such magnetic behavior in a layered rare earth compound and the first lanthanide compound with SMM behavior having more than 12 metal centers.[12] However, the relative contribution to this behavior arising from single ion effects, and from the magnetic interactions, both intra and interlayers, has remained unclear. In fact although in general the magnetic interactions of
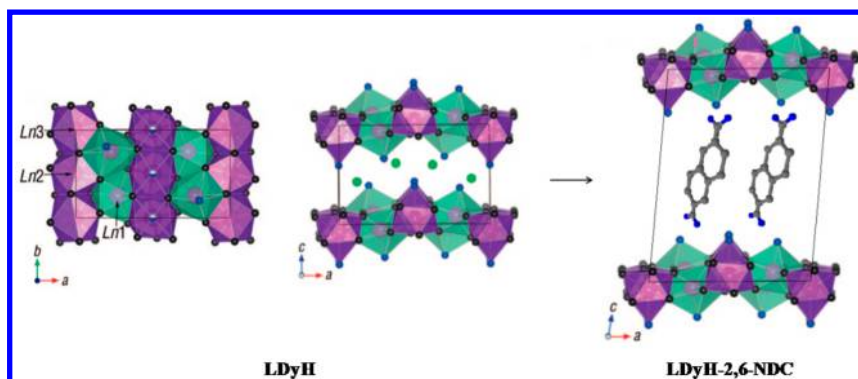
Figure 1. $Ln_8(OH)_{20}Cl_4 \cdot nH_2O$ crystal structure viewed along the c axis (left) and b axis (center) and schematic representation of the LDyH-2,6-NDC structure viewed along the b axis (right). Ln ions are depicted as purple, hydroxyls as gray, water molecules as blue, chloride ions as green, and carbon as gray balls. The 8-fold dodecahedron and 9-fold monocapped square antiprism are in light green and purple, respectively (adapted from ref 6).

lanthanide ions with neighboring magnetic species are rather weak due to the inner character of 4f-electrons, the LDyH presents in each layer of the structure a dense network of Dy–Dy contacts at relatively short distances, both direct and mediated by bridging O atoms. Consequently, the magnetic anisotropy might have a non-negligible contribution from the Dy–Dy interactions in the layers. The interlayer interactions may also be not negligible.

With the aim of distinguishing between these contributions, in this Article we report a study on the Dy compound both diluted in the diamagnetic Y analogous matrix, and intercalated with 2,6-naphthalene dicarboxylate anions (LDyH-2,6-NDC). The first will show the behavior of the single Dy ions, while the intercalated material is expected to reveal the effects of isolated layer (purely 2-D) interactions. Semiempirical calculations using a radial effect charge model for the crystal field splitting of the Dy levels are used to explain data in terms of contributions from the different Dy sites.

EXPERIMENTAL SECTION

Materials. The starting materials $DyCl_3 \cdot 6H_2O$ (Aldrich), $YCl_3 \cdot 6H_2O$ (Aldrich), NaCl (Panreac), hexamethylenetetramine (HMT) (Aldrich), and 2,6-naphthalenedicarboxylic acid (Aldrich) were obtained from commercial sources and used as received.

Synthesis. The solid solution of layered yttrium hydroxide material doped with 3.85% Dy, abbreviated for simplicity as LYH:0.04Dy, was prepared following a previously reported procedure for LDyH using instead a mixture of Y and Dy salts.[6] The intercalated material (LDyH-2,6-NDC) was prepared by hydrothermal anion exchange.

LYH:0.04Dy. A mixture of $YCl_3 \cdot 6H_2O$ (1.440 g; 4.75 mmol), $DyCl_3 \cdot 6H_2O$ (0.094 g; 0.25 mmol), NaCl (3.799 g; 65 mmol), and HMT (0.701 g; 5 mmol) was dissolved in 1000 cm^3 of decarbonated Milli-Q water, and the solution was heated at refluxing temperature overnight under continuous magnetic stirring and nitrogen gas protection. The final product was recovered by filtration and washed with decarbonated distilled (DD) water and the solid dried at room temperature under reduced pressure. Anal. Calcd for $Y_{7.692}Dy_{0.308}(OH)_{20}Cl_4 \cdot 6H_2O$: Dy, 3.77; Y, 51.62; H, 2.43%. Found: Dy, 3.78; Y, 51.63; H, 2.75%.

LDyH. $Dy_8(OH)_{20}Cl_4 \cdot 5H_2O$ was prepared as above but using $DyCl_3 \cdot 6H_2O$ (1.885 g; 5 mmol), NaCl (3.799 g; 65 mmol), and HMT (0.701 g; 5 mmol) for the reacting mixture. Anal. Calcd for $Dy_8(OH)_{20}Cl_4 \cdot 6H_2O$: Dy, 68.78; H, 1.71%. Found: Dy, 68.58; H, 1.93%.

LDyH-2,6-NDC. 2,6-Naphthalene dicarboxylic acid was deprotonated with a solution of NaOH, 50% in water, and if necessary, pH was adjusted to 7 with a diluted solution of HCl. Excess (3 equiv) of 2,6-naphthalene dicarboxylate was added to a suspension of LDyH in DD

water and stirred for about 20 min. The mixture was sealed in a 25 mL Teflon-lined stainless-steel autoclave and kept at 100 °C for 12 h. The reaction mixture was then cooled to room temperature, and the product was recovered by filtration, washed with DD water, and dried at room temperature under reduced pressure. Anal. Calcd for $Dy_8(OH)_{20}(C_{12}H_6O_4)_2 \cdot 6H_2O$: Dy, 59.73; C, 13.24; H, 2.04%. Found: Dy, 59.80; C, 13.65 H, 2.42%.

Characterization Procedures. Microanalyses for C and H were performed on a CE Instruments EA1110 automatic analyzer. To guarantee complete combustion of the samples, V_2O_5 was added during the analysis. Dy and Y were determined by ICP-AES at Laboratório de Análises, Faculdade de Ciências e Tecnologia da Universidade Nova de Lisboa. FT-IR spectra (range 4000–400 cm^{-1}) were collected as KBr pellets using a Jasco FT/IR-4100 spectrophotometer. Conventional XRPD data were collected at room-temperature on a Panalytical X'Pert Pro diffractometer, with a curved graphite monochromator (Cu Kα radiation, λ = 1.540 60 Å), and a flat-plate sample holder, in a Bragg–Brentano para-focusing optics configuration (45 kV, 40 mA). Samples were step-scanned in 0.01° 2θ steps with a counting time of 2 s per step

Magnetic Characterization Measurements. Magnetic susceptibility measurements were performed on fixed powder polycrystalline samples of about 35 mg using a 6.5 T S700X SQUID magnetometer (Cryogenic Ltd.). Direct current susceptibility data measurements were performed at temperatures ranging from 1.7 to 300 K, under applied magnetic fields up to 0.1 T. Alternating current measurements were taken using a MagLab 2000 system (Oxford Instruments) with an ac field of 5 Oe. Temperature dependence of ac magnetic susceptibility was measured in the 10–10 000 Hz frequency range under a zero and 1000 Oe static field. Additional isothermal ac susceptibility measurements, $\chi_{AC} = f(\omega)$, were taken in the 10–10 000 Hz frequency range, within 1.7 and 12 K. All the data were corrected for diamagnetic contributions from the core diamagnetism estimated using Pascal's constants ($\chi_D = -361.9 \times 10^{-6}$ emu/mol, $\chi_D = -315.6 \times 10^{-6}$ emu/mol, and $\chi_D = -561.8 \times 10^{-6}$ emu/mol for LDyH, LYH:0.04Dy, and LDyH-2,6-NDC, respectively).

RESULTS AND DISCUSSION

The preparation of the diluted compound LYH:0.04Dy followed a procedure identical to that previously described for LDyH, and the intercalated compound LDyH-2,6-NDC was obtained using a procedure adapted from that previously described for the Eu analogue,[13] both with similar yields. The elemental analyses are in good agreement with the calculated values for the target diluted $Y_{7.692}Dy_{0.308}(OH)_{20}Cl_4 \cdot 6H_2O$ (LYH:0.0385Dy, abbreviated as LYH:0.04Dy), and intercalated $Dy_8(OH)_{20}(C_{12}H_6O_4)_2 \cdot 4.5H_2O$ (LDyH-26-NDC) materials, with Dy:Y ratio, as determined by ICP-AES, closely following

the starting reaction solution ratio, as expected in view of similar ionic radius and chemical behavior. The powder X-ray diffraction pattern of the LYH:0.04Dy (Figure S1 in Supporting Information) shows sharp and intense peaks comparable to the undiluted material LDyH, confirming the high crystallinity and the formation of a solid solution between the Dy and Y compounds. SEM observations confirm an identical plate shaped crystal morphology in both pure and diluted samples with typical dimensions $0.1 \times 0.5 \times 1 \ \mu m^3$.

The intercalated LDyH-2,6-NDC material presents in the powder X-ray diffraction pattern (Figure S1 in Supporting Information) peaks broader than the precursor, denoting a decrease of crystallinity as often observed in intercalated materials with large organic anions which may easily induce interlayer disorder. The intercalation is clear in the powder diffraction patterns due to the appearance of a new diffraction maximum compatible with interlayer distance increase from 8.4 to 14.8 Å as previously observed in the Eu doped ZnAl layered double hydroxide.[14] The diffraction pattern cannot be indexed in an orthorhombic space group and is instead compatible with a monoclinic group, possibly due to a sliding of the layers as often observed in other hybrid LLHs[7,13] and schematically represented in Figure 1. The presence of the deprotonated form of the intercalated ligand was confirmed by FT-IR analysis (Supporting Information Figure S2), where one can observe the absence of a band around 1695 cm^{-1} ascribed to the $\nu(C=O)$ vibration of the carboxylic acid group of the free ligand and the appearance of two new IR bands at 1560 and 1360 cm^{-1} for the intercalated LDyH-2,6-NDC, which are ascribed to the $\nu_{asym}(OCO^-)$ and $\nu_{sym}(OCO^-)$ vibrations of the deprotonated carboxylate groups, respectively.

■ MAGNETIC MEASUREMENTS

Both diluted and intercalated materials present a perfect overlapping of zero-field-cooled (ZFC) and field-cooled (FC) magnetization curves with no indication of any ordering down to 2 K as previously described for pure LDyH.[11] As seen in Figure 2, the room temperature μ_{eff} values for Dy atom for LYH:0.04Dy and LDyH-2,6-NDC are comparable to that of the pure LDyH compound and close to the expected value of 10.6 μ_B/Dy for 1 noninteracting Dy(III) ion ($S = 5/2$, $L = 5$, $J = 15/2$, $^6H_{15/2}$, and $g = 4/3$). In all compounds there is a
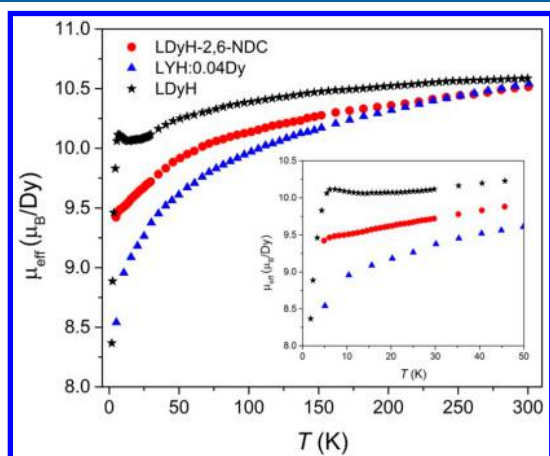
gradual decrease of μ_{eff} upon cooling, with no signs in the diluted compound of the sharp maxima observed in the pure LDyH. A reminiscence of this peak is observed in intercalated material as a small anomaly.

The general decrease of χT (χ is the magnetic susceptibility and T the absolute temperature) upon cooling of these compounds can be understood as resulting from a progressive depopulation of excited Stark sublevels due to the ligand field, as commonly observed in lanthanide compounds.[15] Such a pure single ion behavior is only approached in the Y diluted sample LYH:0.04Dy, and the other samples present a slower χT decreasing rate due to an additional contribution from Dy−Dy interactions which are predominantly ferromagnetic. Assuming a random distribution of the diluted Dy atoms and taking into account that each Ln site has 6 nearest neighbors, 79.0% of Dy atoms are isolated, and 19.0%, 1.9%, and 0.1% have one, two, and three Dy atoms as neighbors, respectively, with virtually no presence of more dense configurations.

In the case of the pure Dy compound LDyH the Dy−Dy interactions lead to a maximum in χT at ca. 6.5 K as previously pointed out.[11] The intercalated material also presents a slower decrease of χT upon cooling, comparable to the precursor LDyH, but however without the maximum at low temperatures. There is a small anomaly at 7.5 K (inset of Figure 2) which may be indicative of a small amount of nonintercalated material or, most likely in view of the slightly different temperature, an intrinsic effect.

The dominant ferromagnetic interactions between the Dy^{3+} ions in a layer can be explained by the highly dense, almost hexagonal, 2D lattice of Dy−Dy contacts. The unit cell contains three crystallographically distinct Dy atoms connected by different types of Dy−Dy contacts bridged by oxygen atoms (from the hydroxyl ligands), with each hydroxyl group acting as a μ_3-bridge between Dy ions, and in three cases the distances are very short (below 3.9 Å), denoting possible direct Dy−Dy interactions.[6,12] The predominant ferromagnetic character of these interactions is in agreement with the fact that the Dy−O−Dy angles are essentially close to 90° leading to near orthogonality of the magnetic orbitals. An analysis of the crystal structure[6] reveals that, out of the different 45 Dy−O−Dy angles in the unit cell, 16 are in the range 93−96°, 15 are between 101° and 103°, and 14 are in the range 110−114°.

Considering the magnetic dependence of the magnetization at 1.7 K, we observe that above 20 kG both for the intercalated and for the diluted material the magnetization is near 5.0 μ_B/Dy μ_B (Figure 3). This value, as already reported for the precursor LDyH, is far from the expected saturation value for a free Dy^{3+} ion (10 μ_B per Dy^{III} ion). This difference can be explained by the magnetic anisotropy of the compounds.[16,17] The magnetization curves of LYH:0.04Dy present no sign of the two step process of the pure LDyH previously ascribed to metamagnetism and spin canting.[11] The magnetization curves of LYH:0.04Dy present hysteresis only at 0.33 K (Figure 3b), however with no coercivity and only under applied fields, which can be due to an efficient quantum tunneling mechanism for the magnetization relaxation occurring at zero field, probably caused by low symmetry components of the crystal field, as it was already observed in other lanthanides compounds.[18] The observed opening of the hysteresis loop at nonzero fields reveals strong field dependence and is due to the suppression of QTM under a magnetic field.

For both diluted and intercalated compounds, the absence of a clear saturation of the magnetization suggests the presence of

Figure 2. Effective magnetic moment of the dysprosium compounds in the temperature range 5−300 K obtained under a magnetic field of 100 G.
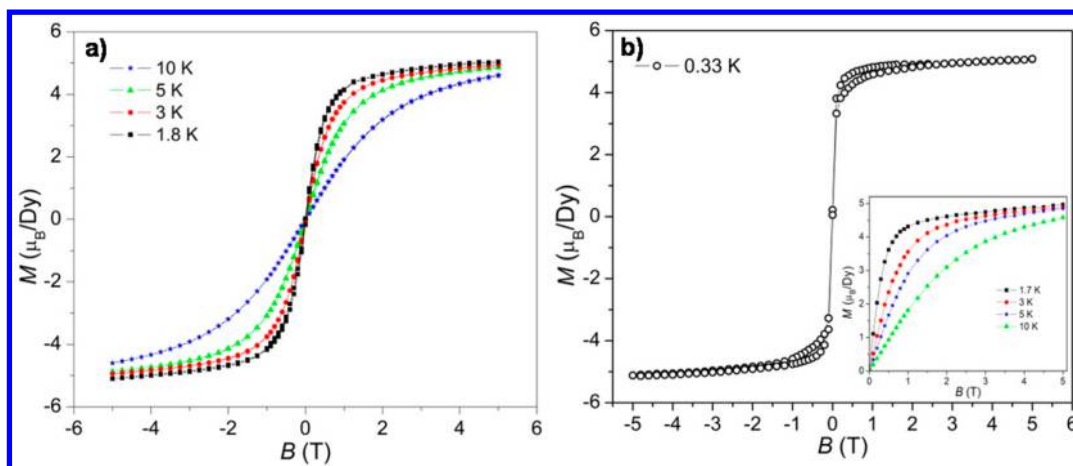
Figure 3. Field dependence of the magnetization at several temperatures for (a) LDyH-2,6-NDC and (b) LYH:0.04Dy compounds.
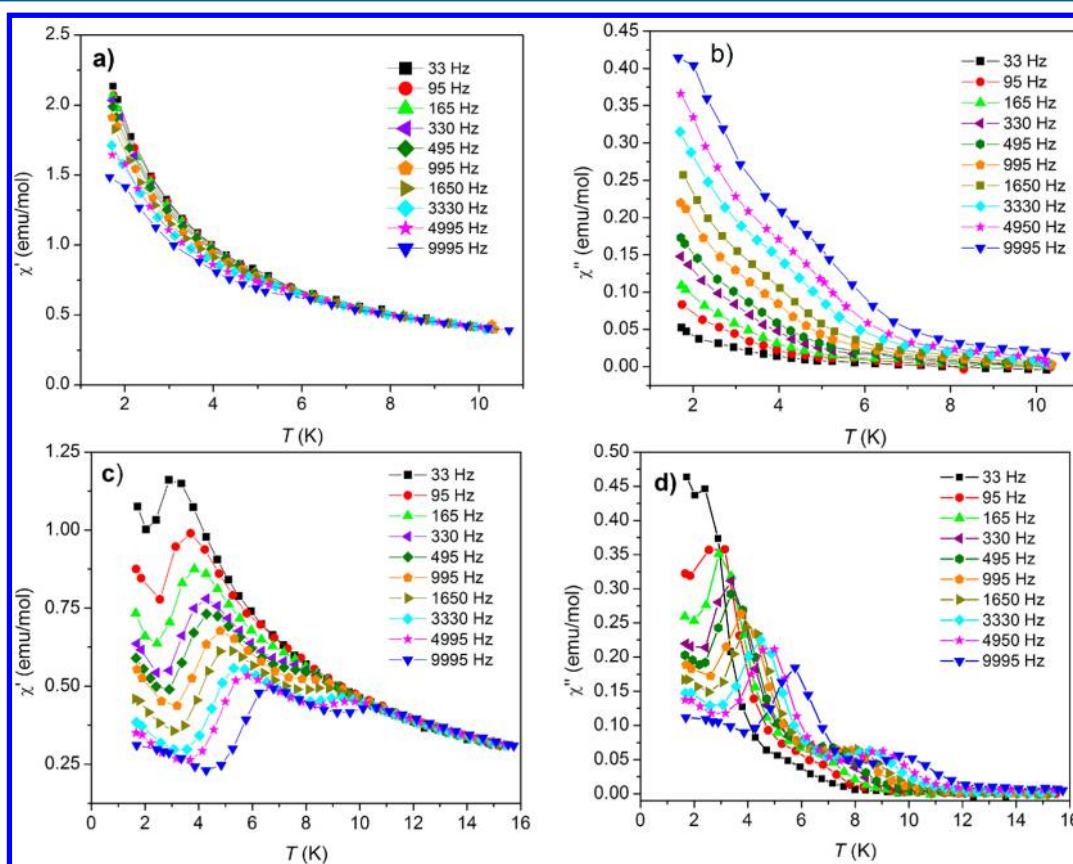
Figure 4. Temperature dependence of the real, χ', and imaginary, χ'', components of the ac susceptibility for LYH:0.04Dy under different static fields, $B = 0$ G (a and b) and $B = 1000$ G (c and d), measured at different ac frequencies.

significant magnetic anisotropy and/or low-lying excited states which was further confirmed by the nonsuperimposition of the M vs B/T curves (Supporting Information Figures S3 and S4). LDyH-2,6-NDC presents down to 1.7 K, the lowest temperature measured, a behavior of the magnetization curves comparable to LYH:0.04Dy.

The magnetization dynamics of both complexes were probed by using ac susceptibility measurements at low temperatures with an ac field of 5 G at different frequency values. The LYH:0.04Dy presents strong frequency-dependent signals below 6 K under both zero (Figure 4a,b) and 1000 G (Figure 4 c,d) static magnetic fields, with the appearance of two

resolved maxima in both real, χ', and imaginary, χ'', components of susceptibility at 1000 G. The intensities of the signals increase with decreasing temperature and frequency. Such performance clearly indicates slow relaxation of the magnetization due to single ion effects originating from two relaxation processes.

These two relaxation processes are most likely associated with the two different types of coordination of the Dy ions in the structure. It should be recalled in this context that the unit cell contains three crystallographically distinct Dy sites, with two different coordination geometries; one (Dy1) presents an 8-fold dodecahedral coordination, $[Dy(OH)_7(H_2O)]$, and two
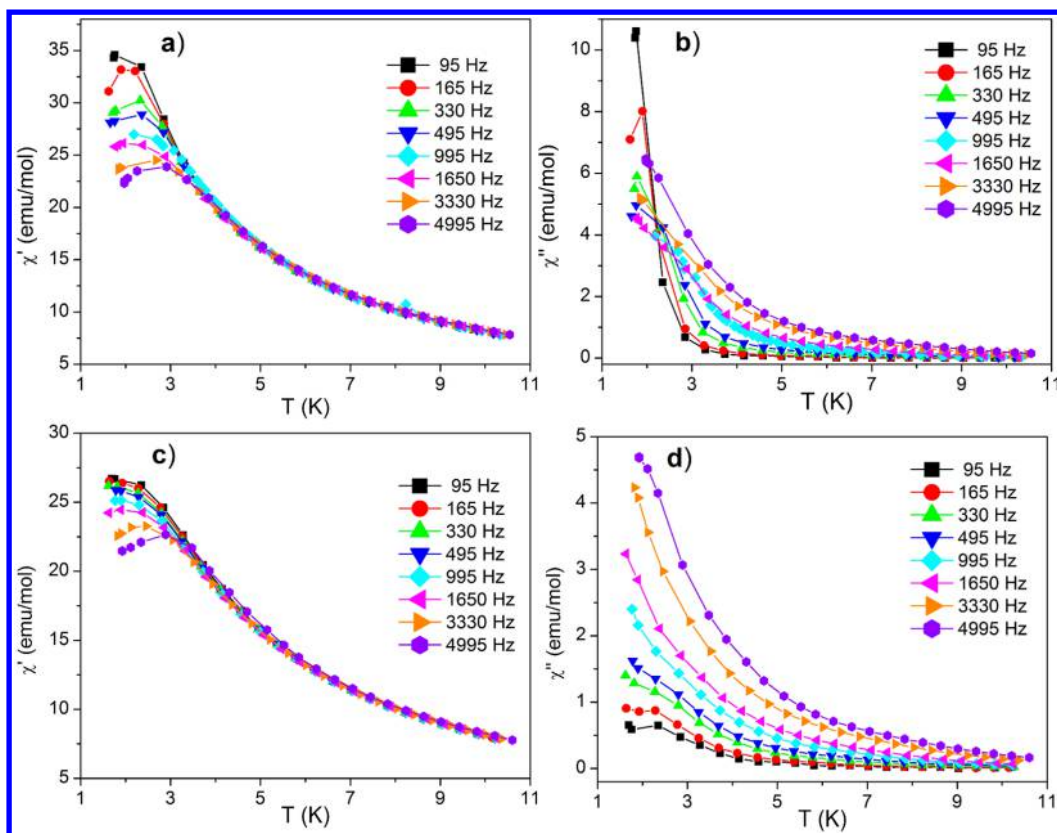
Figure 5. Temperature dependence of the real, χ', and imaginary, χ'', components of the ac susceptibility for LDyH-2,6-NDC under different static fields: $B = 0$ G (a and b) and $B = 1000$ G (c and d), collected at different ac frequencies.

Dy ions (Dy2 and Dy3) present a 9-fold monocapped square antiprism coordination, $[Dy(OH)_8(H_2O)]$. The process at lower temperatures with a more intense ac susceptibility could therefore be ascribed to the $[Dy(OH)_8(H_2O)]$ polyhedron (corresponding to $^2/_3$ of the total Dy^{3+} ions), and the higher temperature one with weaker ac susceptibility would then be associated with $[Dy(OH)_7(H_2O)]$ (corresponding to $^1/_3$ of the total Dy^{3+} ions). It should be noted that in the pure Dy compound only one relaxation process was observed.[11] The absence of two processes of relaxation in the nondiluted LDyH compound is probably due to the ferromagnetic interactions between the Dy ions.

The theoretical calculations by the REC model[19,20] applied to the crystal structure of LYH:0.04Dy using the SIMPRE computational package[21] indicate a different energy level scheme and ground state wave functions for each magnetic center, especially between the two different coordinations of the Dy ions, being compatible with the two different relaxation processes measured that may be attributed to these differences in the coordination environments. For that, the two semi-empirical REC parameters recently reported for the poly-oxotungstate oxygen atoms[22] ($D_r = 0.895$ Å and $Z_i = 0.105$) were used to every oxygen atom coordinating each magnetic center. With this procedure, averaging all three different Dy centers, it was possible to calculate the magnetization curves expected for the diluted sample at different temperatures, which were found in very good agreement with experimental data, as shown in Supporting Information Figure S5. As the shape of the curves was practically coincident with the theoretical prediction, a positive 5% correction was applied to the experimental data for better agreement. Analogously, the

same two parameters were applied to the real crystal structure reproducing quite well the experimental χT product where, in addition to the above-mentioned correction, a TIP of -7.2×10^{-3} emu/mol was introduced (Supporting Information Figure S6).

In order to test the effect of the water molecule of each center, which is chemically different from all the coordinated OH^- and differs more from the polyoxotungstate atoms, the program was run again without considering the water molecule at all (i.e., assuming an effective charge $Z_i = 0$). Results showed that, in this case, the absolute effect of the water molecule is very limited in terms of magnetic properties, energy levels, wave functions, and easy axis orientations.

These calculations show, as expected, that the ground doublet is different for the different crystallographic sites, being composed by 0.76 $|\pm 13/2\rangle$, 0.98 $|\pm 15/2\rangle$, and 0.99 $|\pm 15/2\rangle$, with the g_z values equal to 16.2, 19.79, and 19.91 for Dy1, Dy2, and Dy3, respectively. These results are compatible with the observed SMM behavior with two relaxation processes corresponding to the 8- and 9-fold coordinated Dy ions. Concerning their magnetic easy axis orientation, it was found again that they are very similar in the case of Dy2 and Dy3, but almost perpendicular to Dy1. The easy axes of Dy2 and Dy3 are along the b-axis corresponding to the slightly zigzagging line ($\alpha = 170°$), connecting these ions in the crystal structure. It should be noted that, even in the absence of ferromagnetic superexchange, this alignment of the easy axes is expected to promote a ferromagnetic coupling via dipolar interaction within these spin chains. In contrast, the easy axis of Dy1 is perpendicular to the ab plane. This alignment favors ferromagnetic coupling via dipolar interaction between spin
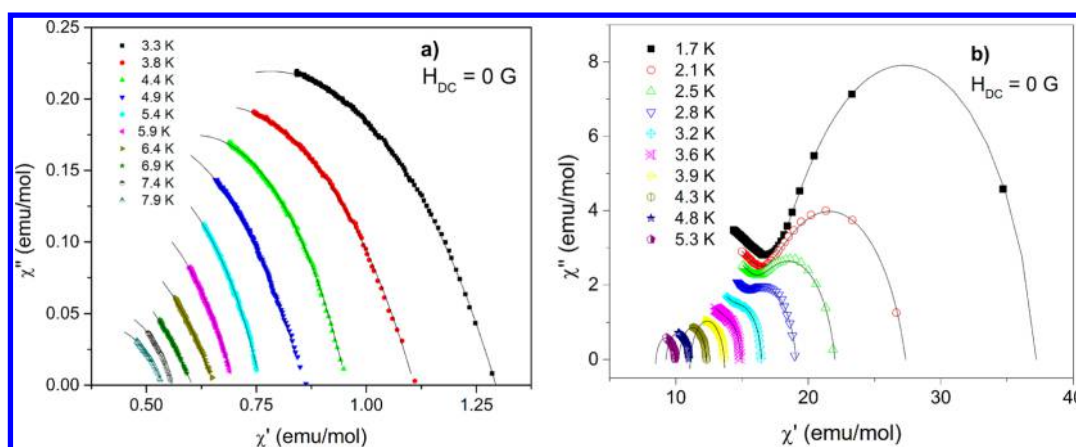
Figure 6. Argand diagrams and Debye fittings of the ac susceptibility for (a) LYH:0.04Dy and (b) LDyH-2,6-NDC at different temperatures indicated. H_{AC} = 5 G; H_{DC} = 0 G.
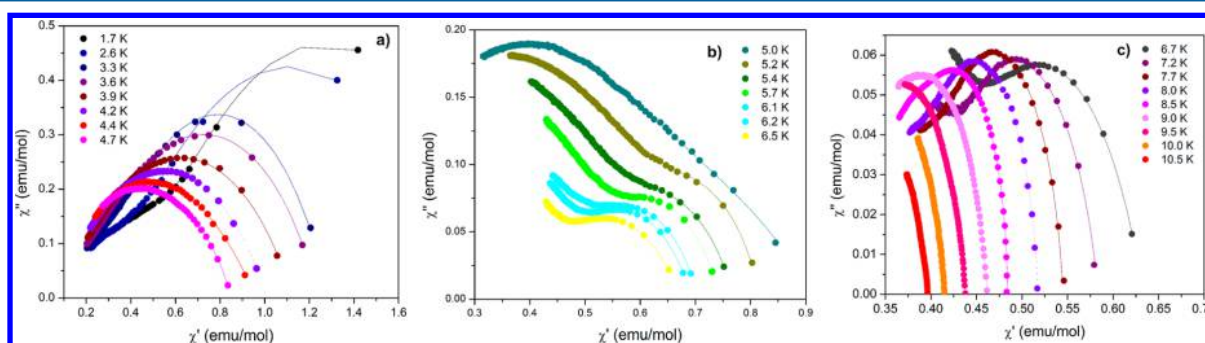
Figure 7. Argand plots and Debye fittings of the ac susceptibility of LYH:0.04Dy in the temperature range 1.7−10.5 K. H_{AC} = 5 G; H_{DC} = 1000 G.

chains of different layers, possibly explaining the slower decrease of effective magnetic moment upon cooling of the nondiluted material as shown in Figure 2. Because of the ferromagnetic superexchange, the near-perpendicular orientation of the easy axes between Dy1 chains and Dy2−Dy3 chains should favor a strongly canted arrangement of magnetic moments with an overall ferromagnetic coupling, both within and between the layers. Such canting arrangement is also denoted by the previously described two-step shape of the low temperature magnetization curve for the undiluted compound.[11]

For LDyH-2,6-NDC, although weaker, the data also reveal a frequency dependence even under zero static field (Figure 5a,b), with single maxima in both χ' and χ'' shifting to higher temperatures with increasing frequencies, following a behavior also characteristic of slow magnetic relaxation.[23] Under a nonzero static field the frequency dependence becomes slightly more pronounced (Figure 5c,d).

In order to further investigate the magnetization relaxation rate, Argand plots were obtained for both compounds from the frequency dependency of ac susceptibility measurements at fixed temperatures and under applied static magnetic fields of zero and 1000 G. At zero static field and for the diluted compound, LYH:0.04Dy (Figure 6a), one distorted semicircle corresponding to a single relaxation process is observed in the range 3−8 K. This data could be well-fitted to a modified Debye model[24]

$$\chi_{total} = \chi_S + (\chi_T - \chi_S)\left[\frac{1}{1 + (i\omega\tau)^{1-\alpha}}\right] \quad (1)$$

where χ_S and χ_T are the adiabatic and isothermal susceptibilities, respectively, τ is the magnetization relaxation time, ω is the frequency, and α is a parameter ranging from 0 to 1 related to the width of the distribution. This fitting gave α values in the range 0.39−0.58 (Supporting Information Table S1). In the case of the intercalated material LDyH-2,6-NDC two distorted semicircles are seen at temperatures below 3.6 K, corresponding to two distinct processes with different relaxation times (Figure 6b). To determine the distribution of relaxation times, for each relaxation mechanism, the ac susceptibility data were fitted on the basis of a linear combination of two processes, 1 and 2, both following modified Debye models

$$\chi_{total} = \chi_S + (\chi_T - \chi_S)\left[\frac{\beta}{1 + (i\omega\tau_1)^{1-\alpha_1}}\right.$$
$$\left. + \frac{1 - \beta}{1 + (i\omega\tau_2)^{1-\alpha_2}}\right] \quad (2)$$

A good fit was obtained with α and τ parameters listed in Supporting Information Table S2, which are within the range expected for lanthanide SIM compounds.

These diagrams are significantly modified with the application of a static magnetic field, which is expected to reduce the quantum tunneling of magnetization (QTM) through spin-reversal barrier via degenerate $\pm M_S$ levels. Both diluted and intercalated compounds show in-phase (χ') and out-of-phase (χ'') signals with a significant frequency dependence in the temperature range 1.7−10 K (Figures 7 and 8 and Supporting Information Figures S7 and S8). For LYH:0.04Dy
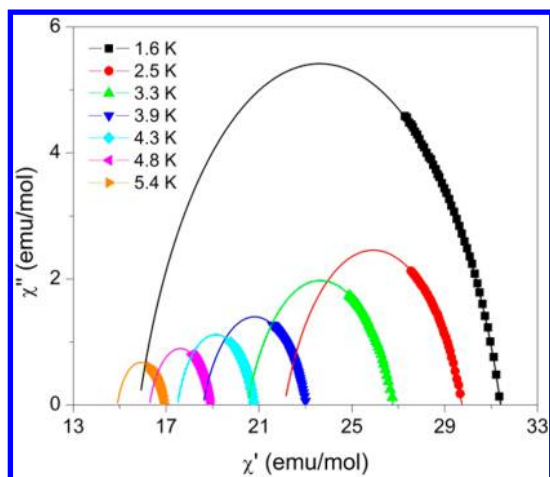
Figure 8. Argand plots and Debye fittings at different indicated temperatures in the range 1.6−5.4 K for LDyH-2,6-NDC. H_{AC} = 5 G; H_{DC} = 1000 G.

two clearly separated distorted semicircles are seen for intermediate temperatures (5.2−8.5 K) corresponding to the two different processes with different relaxation times. For lower and higher temperatures only one semicircle is observed. The distribution of relaxation processes, for each relaxation mechanism, was obtained by a fitting to the linear combination of two modified Debye models of eq 2. The corresponding parameters obtained are presented in Supporting Information Table S3.

For LDyH-2,6-NDC instead of the two relaxation processes that existed under zero static field, only one relaxation mechanism is observed as denoted by single semicircular shapes in all the range 1.6−5.5 K with a fitting to a simple Debye model (eq 1) affording α values in the range 0.22−0.28 (Supporting Information Table S4), which support the existence of a single relaxation process.

From all these data, obtained under both zero and 1000 G static fields, the average magnetization relaxation time τ for each relaxation regime was plotted as a function of temperature between 1.8 and 10 K. The common assumption is naïvely an Orbach process and just performing an Arrhenius law fit, $\tau(T)$ = $\tau_0 \exp(\Delta/k_B T)$, where τ_0, Δ, and k_B are the pre-exponential factor, the relaxation energy barrier, and the Boltzmann constant, respectively. Nevertheless, it is always interesting to check for alternative mechanisms. In particular, in the cases where neither a purely Orbach process nor pure quantum tunneling fit all the data adequately, we perform a fit assuming a Raman process, $1/(\tau)^{1/9} = a+b\cdot T$, i.e., a linear slope in $1/(\tau)^{1/9}$ versus T. The results of these fits can be seen in Figure 9.

Let us analyze the behaviors case by case. In the diluted sample LYH:0.04Dy, as can be seen in Figure 9a,b, a Raman process is at least as likely as a purely Orbach process for the different relaxation mechanisms. In particular, at zero external field one can see a linear slope followed by a horizontal in $\ln(\tau)$ versus $1/T$. This corresponds, at T > 4 K, to an Orbach process, as could be expected from the χ'' versus T data. Thus, we could say that in zero static magnetic field there is only one relaxation regime with an energy barrier of 31 K with τ_0 = 6.84 × 10^{-9} s. This can be compared with the theoretical prediction of energy levels at 35, 77, and 131 K for the three crystallographically different Dy centers. Nevertheless, note that the Raman fit above 4 K (a = 1.6, b = 0.49) is not inferior to the one resulting
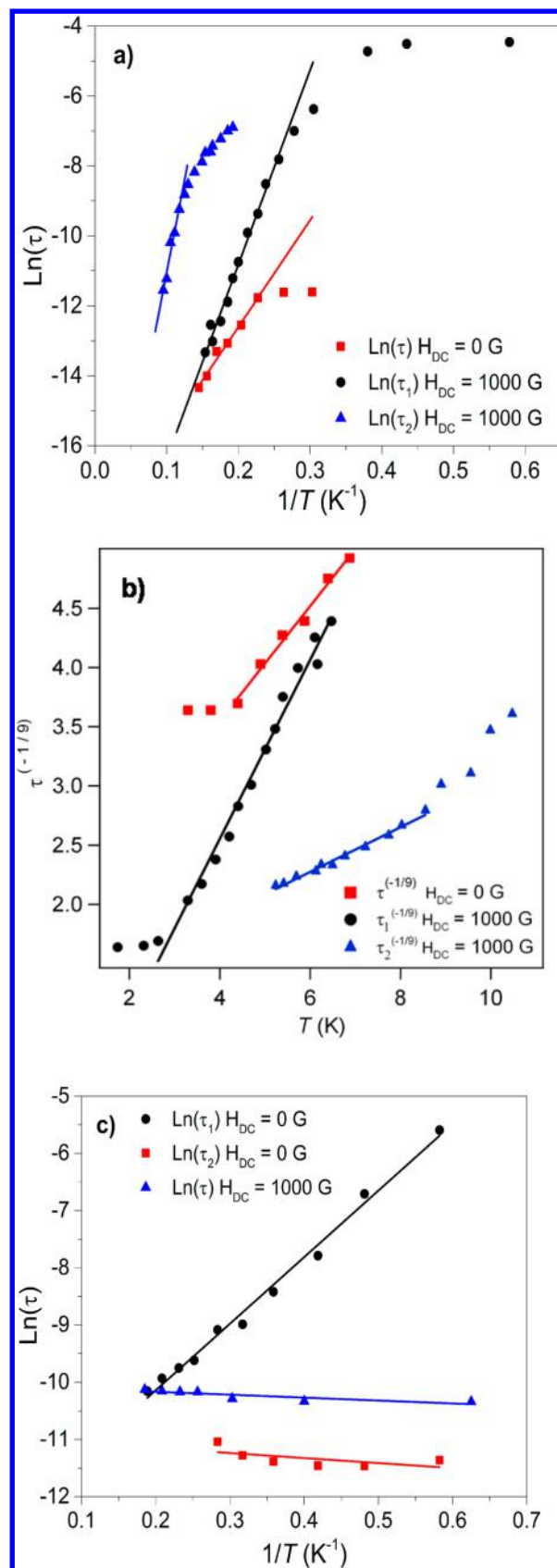
Figure 9. Thermal dependence of the relaxation time measured using ac fields H_{AC} = 5 Oe and static magnetic fields indicated: (a) LYH:0.04Dy at H_{DC} = 0 Oe (red) and H_{DC} = 1000 G (process 2, blue triangles; process 1, black circles). Orbach process assumed (logarithm of the relaxation times versus inverse temperature). (b) LYH:0.04Dy

Figure 9. continued

at H_{DC} = 0 Oe (red) and H_{DC} = 1000 G (process 2, blue triangles; process 1, black circles). Raman process assumed (ninth root of the relaxation frequencies versus temperature). (c) LDyH-2,6-NDC at H_{DC} = 0 G (FR, black circles; SR, red squares) and H_{DC} = 1000 G (blue triangles). Orbach process assumed (logarithm of the relaxation times versus inverse temperature). In all cases, linear fits have been plotted only for the data sets with a significant least-squares result (r > 0.99).

from the Orbach assumption. From 4 K down to 2 K the data are consistent with a temperature independent regime which may result either from spin−spin relaxation or quantum tunneling effects.

When a static magnetic field of 1000 G is applied, the situation is more complicated. For τ_1, there is a short interval at low temperatures where tunneling dominates, and above 3 K either Orbach (U_{eff} = 56 K, τ_0 = 2.79 × 10^{-10} s) or Raman can be assumed (a = −0.47, b = 0.76), with the Raman fit being more adequate to reproduce experimental data at least between 3 and 4 K. In the case of τ_2, Raman (a = 1.14, b = 0.19) and Orbach (U_{eff} = 105 K, τ_0 = 4.60 × 10^{-10} s) fits explain different ranges of the data; the Raman fit is adequate for temperatures below 8.5 K, whereas the Orbach fit is relevant at higher temperatures. This is to be expected, as Orbach processes can only occur when the temperature of the sample is comparable with the temperature of the barrier.

In the case of LDyH-2,6-NDC (Figure 9c) where the layers are more separated, the Arrhenius fits are clearly linear. Nevertheless, the Orbach model can only be applied to the case of τ_1 (in absence of external field), where we find an effective energy barrier U_{eff1} = 11.63 K and τ_1 = 3.86 × 10^{-6} s. The nearly horizontal behavior in the other two cases would be explained by a dominant quantum tunneling at low temperatures (below 5 K), with temperature independent relaxation time τ_2 = 1.72 × 10^{-5} s in absence of field and temperature independent relaxation time τ = 4.26 × 10^{-5} s when a static field of 1000 G is applied.

The larger energy barrier of the diluted sample should be a consequence of suppressing ground-state QTM by magnetic dilution[10] of the Dy^{3+} ions. In the undiluted LDyH and in the intercalated compound LDyH-2,6-NDC, QTM cannot be completely suppressed because the intralayer Dy···Dy distances are very short (smaller than 3.9 Å).[14,25] Note that these unusually short distances correspond to internal fields of the order of 0.5 T, which can produce dipolar interactions of up to 2 cm^{-1}. In fact, these distances are comparable to the ones found in undiluted LiHoF$_4$, which spontaneously orders as an Ising (3D) ferromagnet below 1.5 K.[26]

■ CONCLUSIONS

In this study by comparison of the magnetic properties of the dysprosium layered hydroxide, LDyH, with the Y diluted analogue LYH:0.04Dy and the intercalated compound LDyH-2,6-NDC, we were able to put separately into evidence single ion, and 2D and 3D Dy−Dy interaction effects, which are well-described by semiempirical calculations using a radial effect charge model for the crystal field splitting of the Dy levels. The Y diluted sample LYH:0.04Dy reveals two distinct slow relaxation processes of the magnetization at low temperatures associated with the two main types of Dy sites, 8- and 9-fold coordinated with almost orthogonal orientation of easy

magnetization axes. The easy axes of the $[Dy(OH)_8(H_2O)]$ centers lie along the layers while the easy magnetization axis of $[Dy(OH)_7(H_2O)]$ centers is perpendicular to the layers. The undiluted dysprosium layered compound, LDyH, as well as the intercalated compound LDyH-2,6-NDC present significant Dy−Dy ferromagnetic intralayer interactions and also interlayer in LDyH. Both the dilution and the increase of distance between the layers upon intercalation result in decreased ferromagnetic interactions. As a consequence of the Dy−Dy interactions only one magnetization relaxation process is observed in both undiluted LDyH and intercalated compounds. The ferromagnetic nature of these interactions can be explained by the orientation of the easy magnetization axes of different Dy sites together with the sign of the superexchange interactions expected from the Dy−O−Dy angles.

■ ASSOCIATED CONTENT

⑤ Supporting Information
Powder X-ray diffraction patterns, FT IR spectra, experimental and simulated magnetic data. This material is available free of charge via the Internet at http://pubs.acs.org.

■ AUTHOR INFORMATION

Corresponding Authors
*E-mail: lpereira@ctn.ist.utl.pt.
*E-mail: alejandro.gaita@uv.es.

Author Contributions
The manuscript was written through contributions of all authors. All authors have given approval to the final version of the manuscript.

Notes
The authors declare no competing financial interest.

■ REFERENCES

(1) Leroux, F.; Taviot-Guého, C. *J. Mater. Chem.* **2005**, *15*, 3628−3642.
(2) Wang, Q.; O'Hare, D. *Chem. Rev.* **2012**, *112*, 4124−4155.
(3) Coronado, E.; Mínguez Espallargas, G. *Chem. Soc. Rev.* **2013**, *42*, 1525−1539.
(4) Abellán, G.; Coronado, E.; Martí-Gastaldo, C.; Ribera, A.; Jordá, J. L.; García, H. *Adv. Mater.* **2014**, *26*, 4156−4162.
(5) Geng, F.; Ma, R.; Matsushita, Y.; Liang, J.; Michiue, Y.; Sasaki, T. *Inorg. Chem.* **2011**, *50*, 6667−6672.
(6) Geng, F.; Matsushita, Y.; Ma, R.; Xin, H.; Tanaka, M.; Izumi, F.; Iyi, N.; Sasaki, T. *J. Am. Chem. Soc.* **2008**, *130*, 16344−16350.
(7) Geng, F.; Ma, R.; Sasaki, T. *Acc. Chem. Res.* **2010**, *43*, 1177−1185.
(8) (a) Hasegawa, Y.; Thongchant, S.; Wada, Y.; Tanaka, H.; Kawai, T.; Sakata, T.; Mori, H.; Yanagida, S. *Angew. Chem.* **2002**, *114*, 2177−2179. (b) Yang, X.; Yu, X.-F.; He, D.-F.; Sun, Z. B.; Cao, Z. J.; Wang, Q.-Q. *Adv. Funct. Mater.* **2011**, *21*, 4388−4396. (c) Yoon, Y.-S.; Lee, B.-I.; Lee, K. S.; Im, G. H.; Byeon, S.-H.; Lee, J. H.; Lee, I. S. *Adv.*

Funct. Mater. **2009**, *19*, 3375−3380. (d) Lechevallier, S.; Lecante, P.; Mauricot, R.; Dexpert, H.; Dexpert-Ghys, J.; Kong, H.-K.; Law, G.-L.; Wong, K.-L. *Chem. Mater.* **2010**, *22*, 6153−6161. (e) Yoon, Y.-S.; Byeon, S.-H.; Lee, I. S. *Adv. Mater.* **2010**, *22*, 3272. (f) Lee, B.-I.; Lee, E.-S.; Byeon, S.-H. *Adv. Funct. Mater.* **2012**, *22*, 3562−3569. (g) Wang, L.; Yan, D.; Qin, S.; Li, S.; Lu, J.; Evans, D. G.; Duan, X. *Dalton Trans.* **2011**, *40*, 11781−11787.

(9) Takamatsu, S.; Ishikawa, T.; Koshihara, S.-y.; Ishikawa, N. *Inorg. Chem.* **2007**, *46*, 7250−7252.

(10) Rinehart, J. D.; Fang, M.; Evans, W. J.; Long, J. R. *Nat. Chem.* **2011**, *3*, 538−542.

(11) Monteiro, B.; Pereira, C. C. L.; Coutinho, J. T.; Pereira, L. C. J.; Marçalo, J.; Almeida, M. *Eur. J. Inorg. Chem.* **2013**, 5059−5063.

(12) Woodruff, D. N.; Winpenny, R. E. P.; Layfield, R. A. *Chem. Rev.* **2013**, *113*, 5110−5148.

(13) Chu, N.; Sun, Y.; Zhao, Y.; Li, X.; Sun, G.; Ma, S.; Yang, X. *Dalton Trans.* **2012**, *41*, 7409−7414.

(14) Gao, X.; Hu, M.; Lei, L.; O'Hare, D.; Markland, C.; Sun, Y.; Faulkner, S. *Chem. Commun.* **2011**, *47*, 2104−2106.

(15) (a) Kahn, M. L.; Sutter, J.-P.; Golhen, S.; Guionneau, P.; Ouahab, L.; Kahn, O.; Chasseau, D. *J. Am. Chem. Soc.* **2000**, *122*, 3413−3421. (b) Kahn, M. L.; Ballou, R.; Porcher, P.; Kahndagger, O.; Sutter, J.-P. *Chem.—Eur. J.* **2002**, *8*, 525−531.

(16) (a) Aldamen, M. A.; Clemente-Juan, J. M.; Coronado, E.; Martí-Gastaldo, C.; Gaita-Ariño, A. *J. Am. Chem. Soc.* **2008**, *130*, 8874−8875. (b) Yang, P.-P.; Gao, X.-F.; Song, H.-B.; Zhang, S.; Mei, X.-L.; Li, L.-C.; Liao, D.-Z. *Inorg. Chem.* **2011**, *50*, 720−722.

(17) Liu, C.-S.; Du, M.; Sañudo, E. C.; Echeverria, J.; Hu, M.; Zhang, Q.; Zhou, L.-M.; Fang, S.-M. *Dalton Trans.* **2011**, *40*, 9366−9369.

(18) (a) Ishikawa, N.; Sugita, M.; Ishikawa, T.; Koshihara, S.-y.; Kaizu, Y. *J. Phys. Chem. B* **2004**, *108*, 11265−11271. (b) Silva, M. R.; Martín-Ramos, P.; Coutinho, J. T.; Pereira, L. C. J.; Martín-Gil, J. *Dalton Trans.* **2014**, *43*, 6752−6761.

(19) Baldoví, J. J.; Borrás-Almenar, J. J.; Clemente-Juan, J. M.; Coronado, E.; Gaita-Ariño, A. *Dalton Trans.* **2012**, *41*, 13705−13710.

(20) (a) Baldoví, J. J.; Cardona-Serra, S.; Clemente-Juan, J. M.; Coronado, E.; Gaita-Ariño, A. *Chem. Sci.* **2013**, *4*, 938−946. (b) Baldoví, J. J.; Clemente-Juan, J. M.; Coronado, E.; Gaita-Ariño, A. *Polyhedron* **2013**, *66*, 39−42.

(21) Baldoví, J. J.; Cardona-Serra, S.; Clemente-Juan, J. M.; Coronado, E.; Gaita-Ariño, A.; Palii, A. *J. Comput. Chem.* **2013**, *34*, 1961−1967.

(22) Baldoví, J. J.; Clemente-Juan, J. M.; Coronado, E.; Duan, Y.; Gaita-Ariño, A.; Giménez-Saiz, C. *Inorg. Chem.* **2014**, *53*, 9976−9980.

(23) Mydosh, J. A. In *Spin Glasses: An Experimental Introduction*; Taylor and Francis Ltd.: London, 1993.

(24) (a) Cole, K. S.; Cole, R. H. *J. Chem. Phys.* **1941**, *9*, 341−351. (b) Aubin, S. M. J.; Sun, Z.; Pardi, L.; Krzystek, J.; Folting, K.; Brunel, L. C.; Rheingold, A. L.; Christou, G.; Hendrickson, D. N. *Inorg. Chem.* **1999**, *38*, 5329−5340.

(25) Blagg, R. J.; Ungur, L.; Tuna, F.; Speak, J.; Comar, P.; Collison, D.; Wernsdorfer, W.; McInnes, E. J. L.; Chibotaru, L. F.; Winpenny, R. E. P. *Nat. Chem.* **2013**, *5*, 673−678.

(26) (a) Hansen, P. E.; Johansson, T.; Nevald, R. *Phys. Rev. B* **1975**, *12*, 5315−5324. (b) Chen, S.-W.; Liu, R.-B. *Sci. Rep.* **2014**, *4*, 4695.